

DISC WALL STRUCTURAL ABNORMALITIES CAN ACT AS INITIATION SITES FOR HERNIATION

K. Wade¹, N. Berger-Roscher¹, V. Rasche^{2,3} and H. Wilke^{1,*}

¹ Institute of Orthopaedic Research and Biomechanics, Trauma Research Centre Ulm (ZTF), Ulm University, Ulm, Germany

² Department of Internal Medicine II, University Hospital Ulm, Ulm, Germany

³ Small Animal MRI, Medical Faculty, Ulm University, Ulm, Germany

Abstract

Both posture and loading rate are key factors in the herniation process and can determine the failure mechanism of the disc. The influence of disc structure on the herniation process has yet to be directly observed, thus the aim of this study was to test the hypothesis that discs containing greater levels of pre-existing disruption would be more vulnerable to herniation when subjected to severe levels of posture and loading.

30 ovine lumbar motion segments were subjected to combinations of 4 loading conditions (0 - 12° flexion, 0 - 9° lateral bending, 0 - 4° axial rotation, 0-1500 N axial compression) for 1000 loading cycles at 2 Hz in a dynamic disc loading simulator. The discs were scanned in an ultra-high field MRI (magnetic resonance imaging, 11.7 T) prior to and following testing.

4 discs herniated and 7 discs suffered nucleus displacement. These discs contained pre-existing defects in the central dorsal annulus. Generally, following testing, discs contained more dorsal annulus disruption, including 7 discs which developed similar characteristic defects although these did not herniate. Overall, more severe complex postures produced more disruption.

While more severe postures such as twisting and bending increased disc damage, these results are probably the first directly showing that naturally occurring defects in the disc can act as initiation sites for herniation. The clinical significance of these findings is that, in principle at least, MRI based techniques could be capable of identifying vulnerable discs, with the obvious caveat that further correlation with clinical techniques is required.

Keywords: Intervertebral disc – herniation, complex loading, annulus fibrosus, intervertebral disc – biomechanics, cells/tissues – intervertebral disc, intervertebral disc – prolapse.

***Address for correspondence:** Prof. Dr Hans-Joachim Wilke, Institute of Orthopaedic Research and Biomechanics, Trauma Research Centre Ulm (ZTF), Helmholtzstraße 14, 89081 Ulm, Germany. Telephone number: +49 73150055320 Fax number: +49 73150055302 Email: hans-joachim.wilke@uni-ulm.de

Copyright policy: This article is distributed in accordance with Creative Commons Attribution Licence (<http://creativecommons.org/licenses/by-sa/4.0/>).

Introduction

Intuitively, it seems logical that some discs will be more vulnerable to suffering herniation than others due to the effects of injuries, congenital defects or degeneration. Indeed, it has been suggested that this may be the reason that herniation is common in middle-aged patients whose discs have a weakened annulus but a highly hydrated nucleus (Adams, 2004) and it is well known that artificial defects can act as initiation sites for herniation or degeneration. However, until very recently it has not been possible to explore the role of naturally occurring pre-existing disc structure on the process of herniation because examining the disc in sufficient detail requires

histological examination, which renders subsequent mechanical testing impossible!

Similarly, both posture and loading rate are known to be key factors in the herniation process (Adams, 2004; Adams and Hutton, 1982; Wilke *et al.*, 2016). Loading rate must be sufficiently rapid to overcome viscoelastic effects and can also determine whether the disc fails in the mid-annulus or the endplate junction. Relatively rapid loading (Consmuller *et al.*, 2012; Dolan and Adams, 1993) was recently shown to render the annulus-endplate junction more vulnerable to failure (Berger-Roscher *et al.*, 2017; Veres *et al.*, 2010b; Wade *et al.*, 2015). Both these modes of failure have been observed clinically (Rajasekaran *et al.*, 2013). Longer term loading,

simulating occupational loading, is known to cause disc wall failure (Adams and Hutton, 1985; Callaghan and McGill, 2001; Gregory and Callaghan, 2011; Yates and McGill, 2011) by disruption and limited nucleus displacement in the inner and mid annulus. This was recently observed at the microstructural level in the ovine disc (Schollum *et al.*, 2018; Wade *et al.*, 2016).

While it is clear that a non-neutral posture is required to prevent the annulus fibres from redistributing applied loading, the roles of each component of posture are yet to be determined. Most of the *in vitro* testing has concentrated on the role of flexion (Adams and Hutton, 1982; Roaf, 1960; Veres *et al.*, 2009; Wade *et al.*, 2014), due to the difficulties of applying each component independently. While it was shown by Adams that torsion alone could not cause disc failure due to the limiting influence of the facet joints (Adams and Hutton, 1981), recent investigations support the hypothesis – originally proposed by Farfan – that torsion does play a role in the failure of the disc (Farfan *et al.*, 1970). Ovine lumbar motion segments, subjected to torsion/flexion and rotational shear/flexion, failed at significantly lower loads and were observed to contain distinctive failure morphologies in which alternating lamellae of the annulus were torn, indicating that one population of lamellae had been preferentially overloaded to failure (Veres *et al.*, 2010a). While a recent study found that complex postures can produce endplate junction failure and annulus failure *in vivo*, with more severe postures being more damaging, disc herniations were not produced due to the relatively low magnitude of loading used (Berger-Roscher *et al.*, 2017).

With these factors in mind, this study aimed to test the hypothesis that discs containing greater levels of pre-existing disruption would be more vulnerable to herniation when subjected to severe levels of posture and loading.

A recently developed 6 degree of freedom (6DOF) dynamic testing machine (Wilke *et al.*, 2016) was used to systematically explore the role of each component of complex posture, in order to identify which components are most harmful. Motion segments were examined in detail before and after loading, using high-resolution magnetic resonance imaging (HR-MRI) in order to determine the influence of pre-existing structure on susceptibility to herniation.

Materials and Methods

Experimental design

30 spinal motion segments were gathered from 6 healthy sheep (age 3 – 5 years) and divided into 5 groups (each $n = 6$); in order to limit the possible influence of vertebral level, the upper and lower lumbar spines were equally represented within the groups. All specimens within a group were from different spines, in order to most randomly distribute any potentially degenerate specimens between the groups.

Preparation

Specimens were frozen and stored at $-20\text{ }^{\circ}\text{C}$ prior to testing. It should be noted that these storage conditions are in line with those used in this field and have been shown to cause negligible degradation of specimen properties (Nachemson, 1960; Panjabi *et al.*, 1985; Smeathers and Joanes, 1988). The dorsal (analogous to posterior in a biped) elements were carefully removed, by sawing through the pedicles immediately anterior to the facet joints, to provide a clear view of the dorsal annulus. Note also that while the dorsal elements were removed, the machine was programmed in order to apply the specified postures about axes passing through the centre of the disc laterally and cranio-caudally, and through the dorsal third of the disc in the ventro-dorsal direction. These were chosen in order to approximate the physiological situation, though it is acknowledged that in reality this varies due to the facet joints and surrounding musculature (Pearcy and Bogduk, 1988; Yoshioka *et al.*, 1990).

Imaging techniques

Discs were non-destructively imaged before and after testing to enable the influence of pre-existing structure on susceptibility to herniation to be determined. Micro-computed tomography (μCT) (Skyscan 1172, Skyscan, Kontich, Belgium) was performed at $34\text{ }\mu\text{m}$ resolution, using a voltage of 100 kV and 100 μA current and an acquisition time of 20 min. For magnetic resonance imaging (MRI) scans, the specimens were thawed at $6\text{ }^{\circ}\text{C}$ overnight prior to scanning. Imaging was performed in an 11.7 T HR-MRI (BioSpec 117/16, Bruker Biospin, Ettlingen, Germany), using an experimental protocol derived from previous experiments (MR method: FLASH, contrast: T1, echo time: 3.5 ms, repetition time: 10.0 ms, resolution: $100\text{ }\mu\text{m}$ isotropic, slice gap: $100\text{ }\mu\text{m}$, FOV: $60\text{ mm} \times 70\text{ mm}$, averages: 1, acquisition time: 15 min) (Berger-Roscher *et al.*, 2015). All data were received with a 40 mm quadrature transmit/receive coil.

Further preparation for testing

Following imaging, the samples were prepared for loading. Screws were placed in the vertebral bodies (3 screws, equally spaced about the central axis of the vertebral body, at least 10 mm below the endplate) to ensure robust fixation of the motion segment in the polymethyl methacrylate (PMMA) embedding resin (Technovit 3040, Heraeus Kulzer, Wehrheim, Germany). The embedded motion segments were then stored at $-20\text{ }^{\circ}\text{C}$. Prior to testing, the specimens were thawed at $6\text{ }^{\circ}\text{C}$ for 12 h. Flanges were fixed to the PMMA to enable sample loading in the 6DOF dynamic testing machine (Wilke *et al.*, 2016) (Fig. 1.).

Test protocols

A compressive load of 130 N (typical spinal load for a standing sheep) was applied for 15 min to precondition the specimens (Reitmaier *et al.*, 2013).

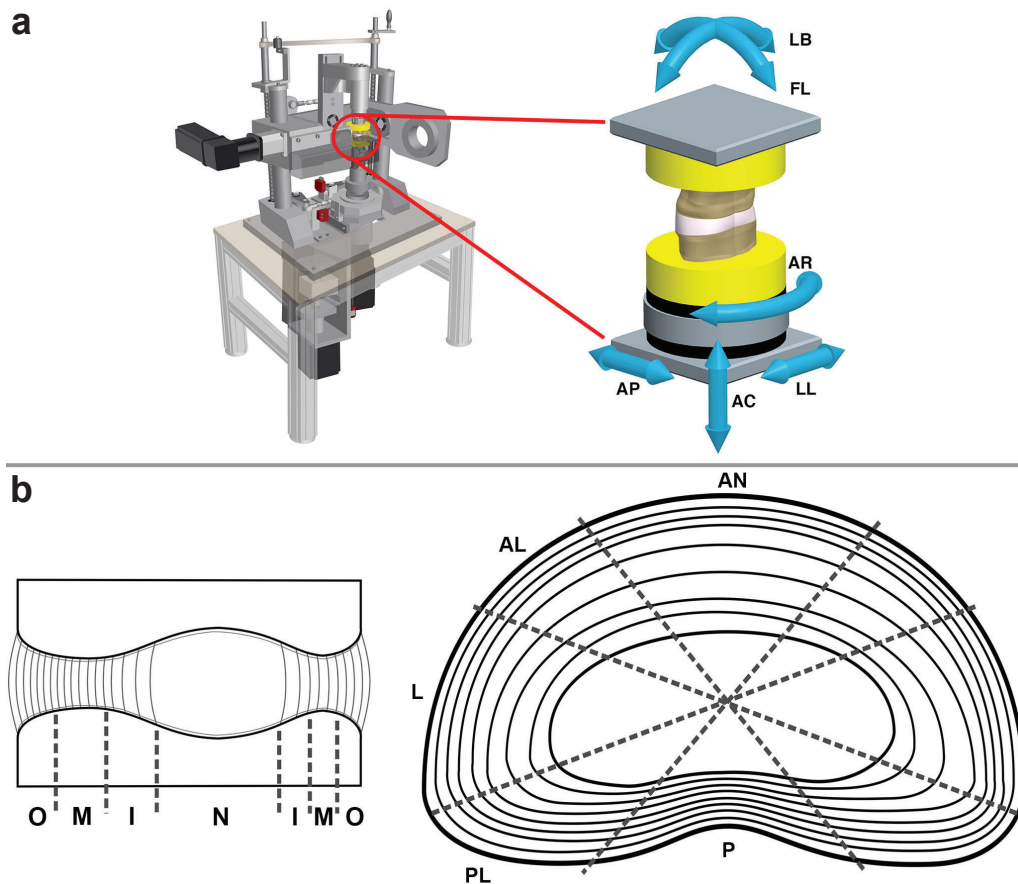


Fig. 1. Experimental setup and terminology. (a) Schematic drawing of the 6DOF dynamic spine tester (left) and a mounted view of the motion segment with each potential direction of motion (FL: flexion; LB: lateral bending; AR: axial rotation; AC: axial compression; DV: dorsal-ventral shear; LL: laterolateral shear) shown. Note that shear was kept fixed during this investigation. (b) Sagittal cross section showing how the disc can be considered as outer annulus (O), mid annulus (M) inner annulus (I) and nucleus (N) Transverse cross section showing how the disc is generally subdivided into ventral (VN), ventrolateral (VL), lateral (L), dorsolateral (DL) and dorsal (D) regions.

Specimens were kept wrapped in dampened gauze prior to testing to maintain hydration (Wilke *et al.*, 1998) and were tested at room temperature, which is also standard practice for short term acute loading (Adams and Hutton, 1982; Wade *et al.*, 2015; Wade *et al.*, 2014; Wilke *et al.*, 2016). Testing was performed using a complex loading protocol (Table 1). The following loading parameters were used: 0 - 13° flexion (FL), 0 - 10° right-lateral bending (LB), and 0 - 4° right-axial rotation (AR) combined with 0 -1500 N of axial compression (AC) at a frequency of 2 Hz, which results in a physiological loading rate (Berger-Roscher *et al.*, 2017; Consmuller *et al.*, 2012; Dolan and Adams, 1993). This posture replicates that used previously by Wilke *et al.* (Berger-Roscher *et al.*, 2017; Wilke *et al.*, 2016) and is double the range of motion (ROM) of ovine lumbar motion segments under 7.5 Nm pure moments applied in each direction (Wilke *et al.*, 1997a). For Groups 1 - 4, during the first 90 cycles, angles were increased in 10 %-increments of the full angle or load with 10 cycles each. For Group 5, each axis was sequentially moved to its maximum, prior to initiation of cyclic loading. Samples were subjected to 1,000 cycles in

total. They were videoed from the dorsal direction to detect visible and audible disc failures. Following testing, the specimens were refrozen at - 20 °C for storage prior to reimaging with μ CT and HR-MRI.

Data analysis

Video documentation and scan images were analysed visually. For image visualisation, ImageJ (U. S. National Institutes of Health, Bethesda, Maryland, USA) was used. Analysis of load-cell data was

Table 1. Overview of the loading conditions applied to each group. FL indicates flexion; LB, lateral bending; AR, axial rotation. Note that groups 1 - 4 had loading applied in 10 % steps over the first 100 cycles of the test while Group 5 was rapidly loaded to the full level of posture sequentially for each axis.

Load component	Group 1 w/o FL	Group 2 w/o LB	Group 3 w/o AR	Group 4 all combined	Group 5 all combined, rapid loading
FL	-	X	X	X	X
LB	X	-	X	X	X
AR	X	X	-	X	X
AC	X	X	X	X	X

conducted using MATLAB (R2013b, The MathWorks Inc., Natick, Massachusetts, USA). Loading curves were synchronised with video documentation and analysed with respect to audible and visible defects. In general, terminology consistent with clinical recommendations was used (Fardon *et al.*, 2014), although these have the limitation of being based on clinical imaging that cannot detect microstructural damage within the disc wall – which necessarily occurs prior to changes at the disc periphery. Given that this investigation was focused on the phenomena leading up to such changes, terminology adopted in similar earlier investigations (Veres *et al.*, 2010a; Wade *et al.*, 2014) was used as appropriate for the present study. Specifically, internal movement of the nucleus, which caused no or minimal distortion of the disc periphery, will be referred to as nucleus displacement and other, less severe, damage to the annular wall will be referred to as defects or disruption as appropriate.

Upon initial examination of the HR-MRI scans of specimens prior to testing, it was immediately apparent that while the motion segments used in this study were taken from relatively young animals that they did contain pre-existing disruption and irregularities and that these were concentrated in the dorsal annulus. The observation of large, coalesced patches of disruption in the central dorsal annulus was of particular interest, and such features were termed defects in the present study. A simple classification scheme for these features was devised in which defects that spanned < 33 % of the annulus were termed small, between 33 and 66 % termed moderate, and greater than 66 % termed large. Discs were evaluated both before and after testing in order to enable correlation between pre-existing structure and post-loading outcomes.

Results

When discs were assessed prior to testing, almost all were found to contain some degree of irregularity in the dorsal (posterior) annulus that was visible using HR-MRI. This corresponds to previous observations of discontinuities in this area. Of key importance to this study was that 11 discs contained some form of defect prior to testing. These defects had a distinctive bell shape, when viewed transversely, similar to that observed by Adams *et al.* (Adams *et al.*, 2000; Adams and Hutton, 1985) whose terminology was used (Fig. 2a) and appeared darker and irregular when compared to the surrounding annulus and nucleus.

Across all groups, 4 discs suffered overt herniation, that is, with extrusion of nucleus material. 2 of these contained large pre-existing defects, 1 contained a moderate pre-existing defect and 1 a small pre-existing defect. Nucleus displacement was observed in a further 7 discs, 6 of which contained a small pre-existing defect and 1 a moderate pre-existing defect. These 11 discs were the same 11 that contained pre-existing defects. Overall, all remaining discs

were affected by the loading to some extent; the pre-existing disruption either became more extensive or coalesced to form a feature similar in appearance to the defects observed prior to testing in the discs which herniated, as summarised in Tables 2 and 3 and described in detail in Tables 4a and 4b. Examples of these features can be seen in Figs. 2 - 5, respectively.

In general, as the severity of the complex posture increased, the level of damage also increased. As in the previous study of Berger-Roscher *et al.* (Berger-Roscher *et al.*, 2017), these failures were accompanied by crackling noises from the discs, which generally occurred between 50 and 100 % of full load, with the exception of the discs tested with immediate application of the full level of posture, which suffered annular failure as flexion was applied. Example videos can be viewed as supplementary information on the paper's parent website. These data are summarised in Table 4.

Mechanical observations

The moment data (summarised in Table 3) was also largely consistent with that of Berger-Roscher *et al.* (Berger-Roscher *et al.*, 2017). Moments in FL were highest, even when the flexion axis was held in neutral. This was expected, given the coupled response of motion segments. The absence of either FL or LB from the complex posture substantially reduced the measured moments (from 40.7 Nm in Group 4 to 24.8 and 22.1 Nm in groups 1 and 2, respectively), corresponding to the large reduction in shape change of the disc. The apparent reduction in moments between groups 4 and 5, which were subjected to all components, is due to the fact that the gradual increase in posture was applied to all axes at once (as in group 4), while the rapid application of maximum posture involved the axes being driven sequentially (as in group 5), with the application of FL always causing dorsal annular failure before the application of LB and AR.

Table 2. Summary HR-MRI observations of the discs before and after loading (based on the new schematic in Fig. 1). Note that the 11 discs that contained some degree of characteristic defect are the 11 discs that had either nucleus displacement or herniation following loading. Of the other discs, the vast majority contained disrupted, irregular lamellae observable by HR-MRI, and this disruption either appeared more extensive or progressed to a characteristic defect following loading. *: Contained endplate fracture afterwards.

Category	Before	After
Regular	1	
Disruption	17	11*
Small defect	7	4
Moderate defect	2	3
Large defect	2	
Displacement		7
Herniation		4

Image analysis

Analysis of the μ CT images showed that the vertebrae were all intact and contained closed growth plates prior to testing. Following testing, one disc had suffered a large vertebral fracture which had deeply penetrated the vertebral body and was filled with nucleus material. However, this was not accompanied by visible herniation or displacement of nucleus material into the annular wall. No substantial fractures were observed in the other discs in this study; although, as in the prior study of Berger-Roscher *et al.* (Berger-Roscher *et al.*, 2017), a large proportion of the discs had suffered

failure of the outer annulus-endplate junction – as judged by observation of small fragments of bone and calcified cartilage that had been displaced in this region (notably Fig. 3f, 4f). However, most of the analysis was focussed on the HR-MRI images since this technique is very well suited to visualising changes in soft tissue.

Examination and correlation of the HR-MRI results revealed that nucleus material had been extruded through the defect regions (Fig. 2a,b) in the central dorsal annulus (Fig. 2d). This was observed in all discs that suffered herniation (Fig. 2) or nucleus displacement which contained a pre-existing defect

Table 3. Summarised loading results for all groups showing pre-existing state of the disc, audible indications of failure, peak moments and overall failure mode of the discs. FL, indicates flexion; LB, lateral bending; AR, axial rotation.

Load component	Group 1 w/o FL	Group 2 w/o LB	Group 3 w/o AR	Group 4 all combined	Group 5 all combined, rapid loading
Regular annulus			1		
Pre existing disruption	3	2	3	5	4
Pre-existing small defect	1	3	2		1
Pre-existing moderate defect	2				
Pre-existing large defect				1	1
Crackling noise (cycle)	71 (70 - 100)	84 (80 - 90)	76 (50 - 90)	70 (30 - 103)	(0)*
Peak moments FL (N.m)	24.8 (15.2 - 42.5)	22.1 (13.3 - 54.3)	37.6 (27.5 - 48.3)	40.7 (24.1 - 58.5)	31.7 (12.8 - 42.9)
Peak moments LB (N.m)	22.1 (19 - 39.1)	16.1 (13 - 23.7)	24.9 (19.5 - 32.9)	19.4 (14.8 - 32.9)	13.3 (10.1 - 23.7)
Peak moments AR (N.m)	14.1 (12.4 - 16.3)	13.2 (9.1 - 14.1)	5 (1.9 - 6.9)	11.8 (9.5 - 16.7)	13.2 (9.1 - 14.1)
New small defect	1		2	1	
New moderate defect			1	1	1
New large defect					
Displacement	2	2	2		1
Herniation	1	1		1	1

Table 4a. Summary of disc morphology before and after loading. Loading regime (see Table 3) shown in brackets in the row labelled “before”. Cycle at failure is indicated by (CY) in the row labelled “after”.

Disc	2453	2495	2496
L1-2	before: minor general disruption (1)	before: minor general disruption (2)	before: small characteristic defect (3)
	after: increased disruption in dorsal AF (CY 103)	after: (No data) (CY 80)	after: displacement (CY 70)
L2-3	before: minor general disruption (2)	before: small characteristic defect (1)	before: small characteristic defect (2)
	after: increased disruption in dorsal AF (CY 80)	after: displacement (CY 30)	after: displacement (CY 90)
L3-4	before: minor general disruption (5)	before: regular annulus (3)	before: moderate characteristic defect (1)
	after: increased disruption in dorsal AF	after: moderate characteristic defect (CY 80)	after: displacement (CY60)
L4-5	before: minor general disruption (4)	before: small characteristic defect (5)	before: large characteristic defect (4)
	after: increased disruption in dorsal AF (CY 90)	after: displacement	after: herniation (CY 86)
L5-6	before: minor general disruption (3)	before: minor general disruption (4)	before: large characteristic defect (5)
	after: increased disruption in dorsal AF (CY 70)	after: increased disruption in dorsal AF (CY 80)	after: herniation

Table 4b. Summary of disc morphology before and after loading. Loading regime (see Table 3) shown in brackets in the row labelled “before”. Cycle at failure is indicated by (CY) in the row labelled “after”.

Disc	2497	2498	2499
L1-2	before: minor disruption in dorsal AF (4)	before: minor disruption in dorsal AF (5)	before: minor disruption in dorsal AF (5)
	after: moderate characteristic defect (CY 82)	after: increased disruption in dorsal AF	after: moderate characteristic defect
L2-3	before: very minor disruption in dorsal AF (3)	before: minor disruption in dorsal AF, Schmorl’s node (4)	before: minor disruption in dorsal AF (1)
	after: small characteristic defect (CY 70)	after: Schmorl’s node got larger, increased disruption in dorsal AF (CY 88)	after: small characteristic defect (CY 60)
L3-4	before: moderate disruption in dorsal AF (2)	before: small characteristic defect (3)	before: minor disruption in dorsal AF (4)
	after: endplate fracture (CY 72)	after: displacement (CY 100)	after: small characteristic defect (CY 80)
L4-5	before: moderate general disruption in dorsal AF (1)	before: small characteristic defect (2)	before: minor disruption in dorsal AF (3)
	after: increased disruption in dorsal AF (CY 80)	after: subligamentous herniation (CY 72)	after: small characteristic defect (CY 72)
L5-6	before: moderate disruption in dorsal AF (5)	before: moderate characteristic defect (1)	before: small characteristic defect (2)
	after: increased disruption in dorsal AF	after: herniation (CY 80)	after: displacement (CY 50)

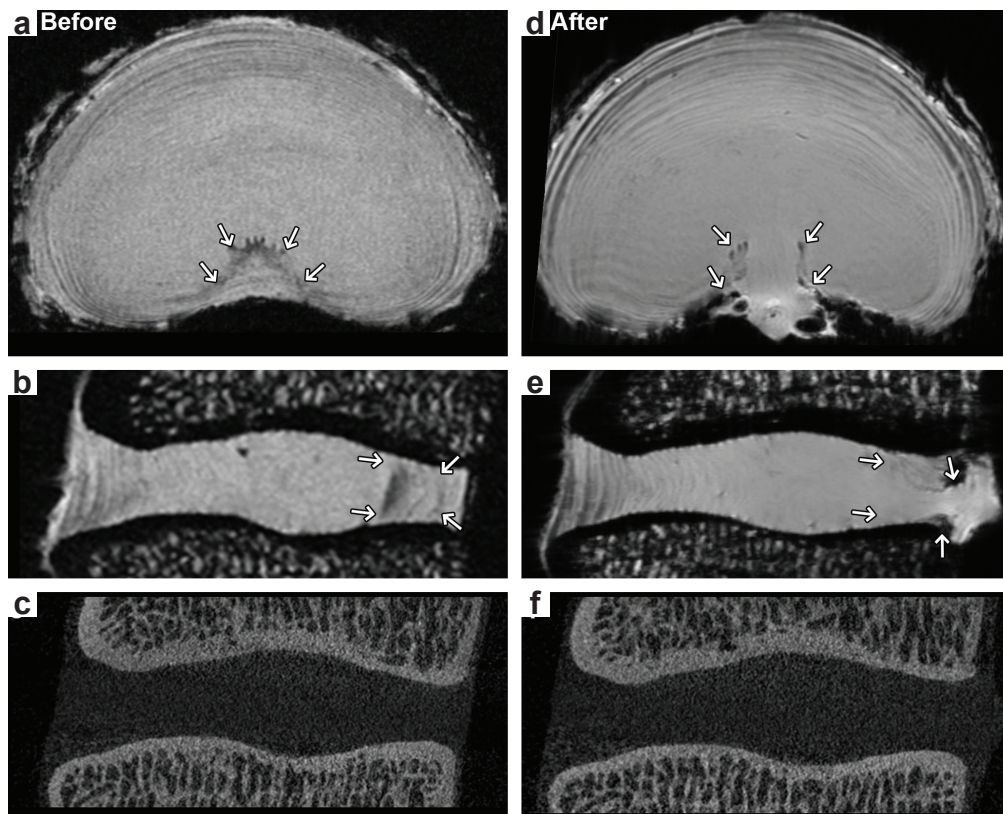


Fig. 2. HR-MRI images from a disc which contained a large characteristic defect before testing. (a) Transverse section. (b) Sagittal section. (c) Corresponding μ CT sagittal section. It had herniated after testing. (d) Transverse section. (e) Sagittal section. (f) Corresponding μ CT sagittal section). The characteristic defect and the herniation are indicated by the arrows.

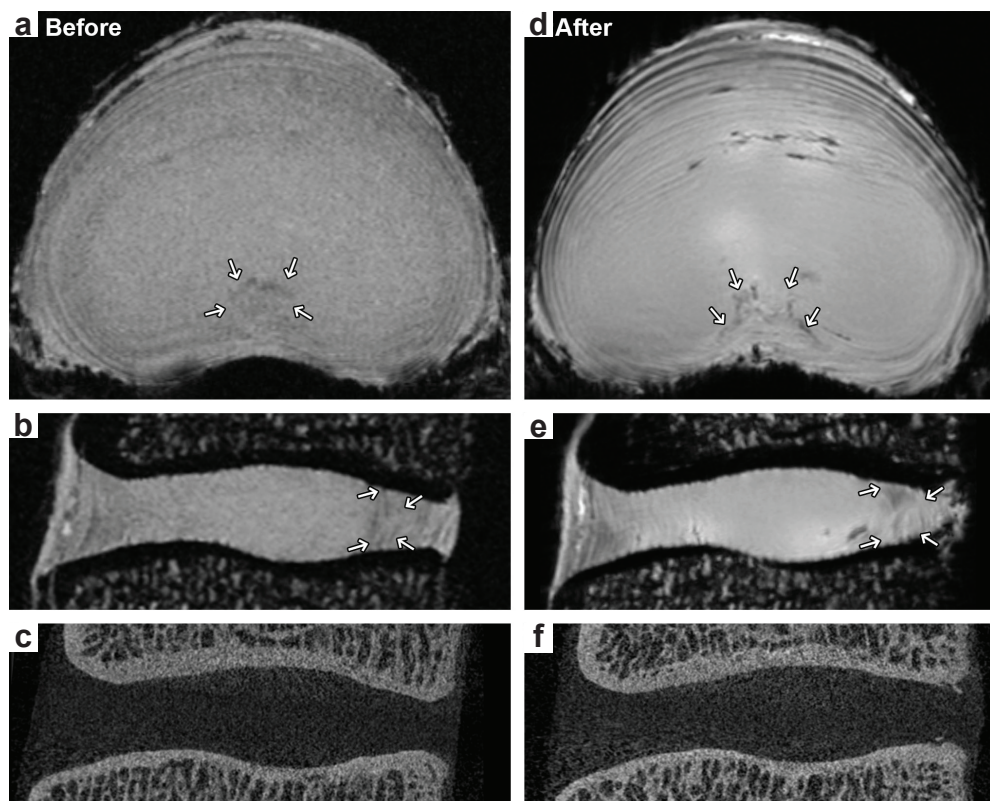


Fig. 3. HR-MRI images from a disc which contained a moderate characteristic defect before testing. (a) Transverse section. (b) Sagittal section. (c) Corresponding μ CT sagittal section. Nucleus displacement shown after testing. (d) Transverse section. (e) Sagittal section. (f) Corresponding μ CT sagittal section. The characteristic defect and nucleus displacement are indicated by the arrows. Small fragments of endplate, likely calcified cartilage, have been displaced in the dorsal annulus following testing as observed by μ CT.

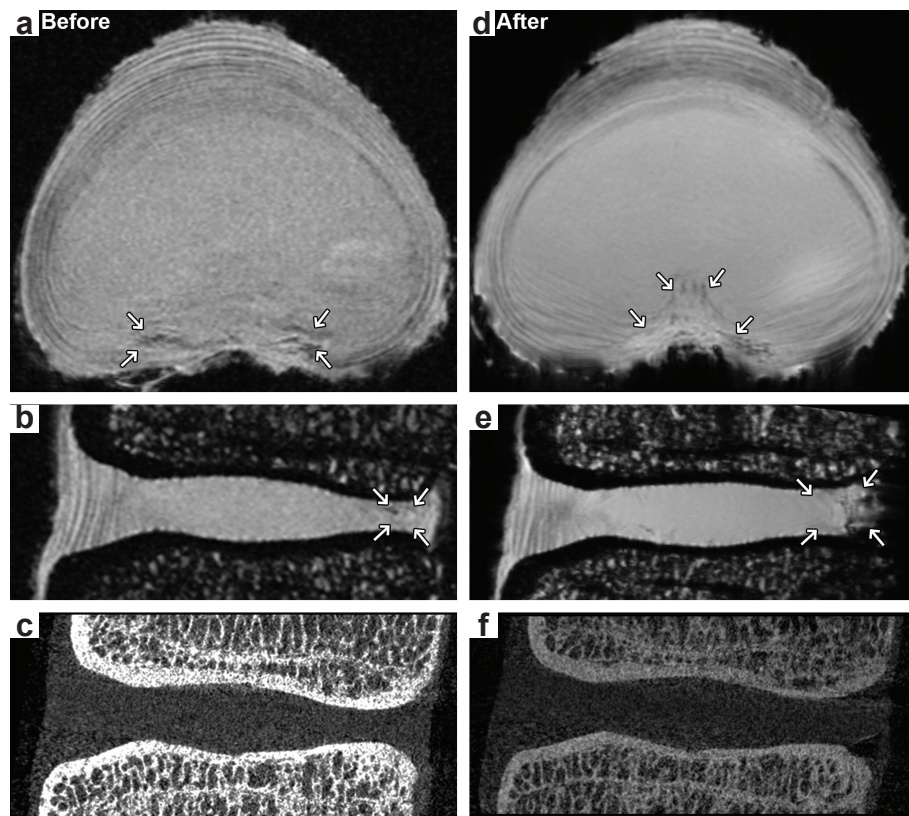


Fig. 4. HR-MRI images from a disc which contained minor disruption in the dorsal annulus before testing. (a) Transverse section. (b) Sagittal section. (c) Corresponding μ CT sagittal section. This had developed a moderate characteristic defect in the central dorsal annulus after testing. (d) Transverse section. (e) Sagittal section. (f) Corresponding μ CT sagittal section. The minor disruption and the characteristic defect are indicated by the arrows.

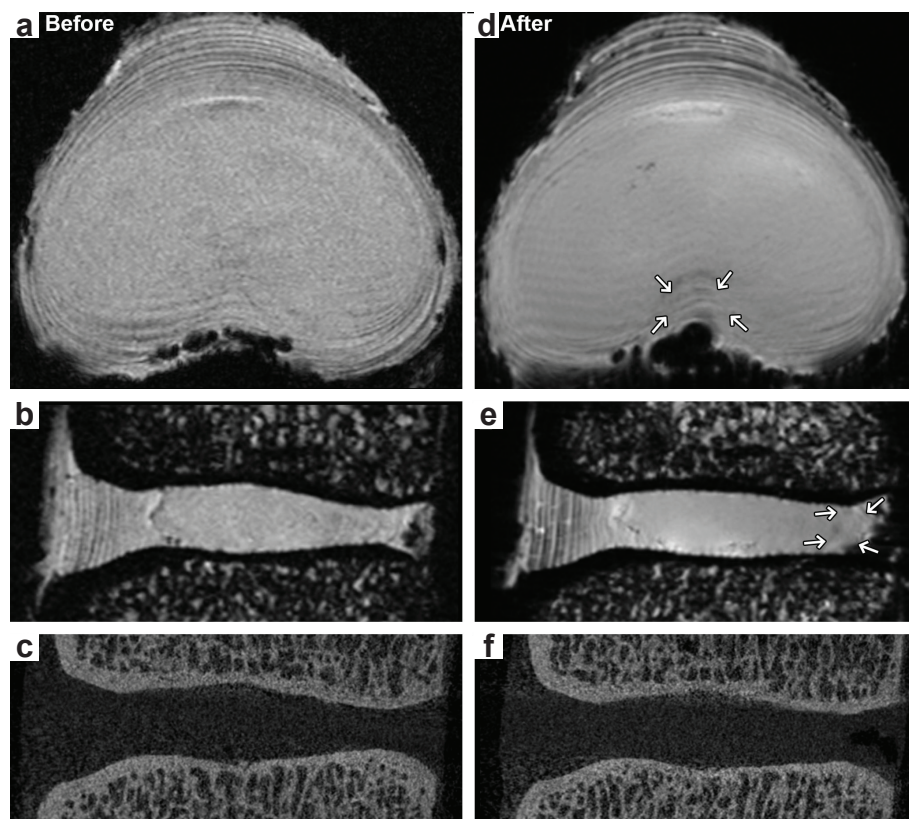


Fig. 5. HR-MRI images from a disc which appeared normal before testing. (a) Transverse section. (b) Sagittal section. (c) Corresponding μ CT sagittal section. This had developed a small characteristic defect in the central dorsal annulus after testing. (d) Transverse section. (e) Sagittal section. (f) Corresponding μ CT sagittal section. Here, the characteristic defect is indicated by the arrows in the post-test images.

(Table 2, 3a,b). Generally, the discs that suffered nucleus displacement contained small pre-existing defects (Fig. 3a,b). These had the same bell shape, but were less pronounced when viewed in transverse section (*cf.* Fig. 2a, 3a). Nucleus material had been displaced into this defect when the pre- and post-test images were compared (Fig. 3a,d).

The discs that did not suffer herniation or nucleus displacement contained minor irregularities in the dorsal annulus prior to testing. Importantly, these did not appear to substantially disturb the overall arrangement of the dorsal annulus lamellae when viewed in transverse section (examples in Fig. 4a, 5a). However, following testing, both these discs contained bell-shaped defects (Fig. 4d, 5d) similar to those in the pre-test images (see Fig. 2a, 3a). These were not present prior to testing, indicating they developed as a consequence of the loading the disc was subjected to. In total, 7 discs developed such defects, as observed under HR-MRI. The remainder were observed to contain increased disruption in the dorsal annulus (Table 3a,b).

Discussion

These results clearly show that disc structure has determined the behaviour of the disc under these loading conditions, since all 11 discs that contained a pre-existing defect were the same 11 that suffered herniation or nucleus displacement. The remainder of the discs in this study did not contain these distinctive bell-shaped defects prior to testing and did not suffer herniation or nucleus displacement, though these discs did contain greater levels of disruption following testing. Thus, it was not possible to determine precisely what component of the complex postures tested here was most harmful, beyond making the general observation that more severe postures are more damaging to the disc, which is in agreement with other recent *in vitro* experiments in this area (Berger-Roscher *et al.*, 2017; Shan *et al.*, 2017; Veres *et al.*, 2010a; Wade *et al.*, 2017). Nonetheless, to the authors' knowledge, this is the first study to report in detail how naturally occurring variations in disc structure behave when subjected to acute overloading. It should also be noted that the age of the animals in this study was consistent with other investigators, who assumed that they represent mature healthy discs (that is, Grade I-II by most measures). Similarly to these previous studies, the discs in the present study did not contain signs of severe degeneration, such as brown or yellow discolouration, when bisected cranio-caudally and examined macroscopically following testing and scanning. This suggested that while the discs contained pre-existing irregularities (as described in Tables 3, 4a,b), and have been affected by the loading they have been subjected to in the present study, they had not undergone the biochemical changes associated with the later stages of degeneration.

With this in mind, the key finding from the present study was that only discs that contained pre-existing bell-shaped defects suffered herniation or nucleus displacement. This suggested that these pre-existing characteristic defects act as initiation points for nucleus displacement and herniation, at least under these loading conditions. The central dorsal location of these characteristic defects corresponded to the direct dorsal path of both the herniations and nucleus displacement observed in the present study. A recent finite-element analysis (FEA) investigation, exploring the effects of these very same postures on ovine discs, reports that this central dorsal region is generally highly stressed under all postures investigated (Casaroli *et al.*, 2017). Postures combining FL, LB and AR did differentially stress one side of the annular wall, in addition to this central dorsal region. Similar findings have been observed previously in simulations of human discs (Schmidt *et al.*, 2007a; Schmidt *et al.*, 2007b).

How might these defects occur?

This provides an explanation for the presence of pre-existing defects in the samples used in the current study – it follows that mechanical damage would tend to accumulate in the most highly stressed region of the annular wall during life! However, it is acknowledged that it is possible that congenital defects such as incomplete lamellae may also be present in this area, and could potentially interact with the effects of mechanical loading. It is also notable that the most severe pre-existing defects were found in discs from the lower lumbar levels in 2 particular spines (see Table 3). This suggested that sheep may also suffer the more severe disc damage and degeneration in their lower lumbar discs as is observed clinically in humans (Ebeling and Reulen, 1992; Moore *et al.*, 1996). An individual susceptibility can also be evoked, as not all individuals are affected in the same way. Given the age of the animals (3 - 5 years old) it is suggested that these discs, which have been shown to be most vulnerable to acute overloading in human tissue (Adams, 2004), were in the early stages of degeneration. However, it should be noted that these previous studies did not directly image the mechanism by which this degeneration weakened the discs! That characteristic defects were produced by the loading regimes (see Table 3, 4a,b and Fig. 4d, 5d) is consistent with the FEA findings described above and implies that mechanical loading is implicated in the development of these characteristic defects and thus the development of early stage degeneration.

How do these defects weaken the disc?

Overall, these results suggested that the process, by which these characteristic defects can lead to herniation, is that long-term exposure to loading causes disruption of the central dorsal region at a greater rate than the disc can repair itself – given the matrix turnover rates of several years or more

(Kandel *et al.*, 2008; Sivan *et al.*, 2014). Over time, this damage accumulates and forms a characteristic defect. If subjected to acute traumatic loading when accompanied by high pressure in the nucleus, the nucleus migrates into the defect, potentially leading to herniation (Fig. 6).

Given that the applied loading produced features very much like the pre-existing characteristic defects (*cf.* Fig. 2a, 3a *vs.* Fig. 4d, Fig. 5d), it must be explained why only those discs with pre-existing features herniated. Because of the nature of these *in vitro* tests, there would not have been any cell activity during testing. Given current research into the behaviour of disc cells, showing that they react to their environment (Neidlinger-Wilke *et al.*, 2014), it seems likely that biological processes would be involved in the development and progression of the defects. It is also possible that the testing regime used dehydrated the nucleus in the early stages of loading, reducing its potential to generate pressure when the more extreme postures were applied in the latter stages of the test. This would reduce the susceptibility of the disc to herniation, as has been suggested previously in literature (Adams, 2004).

The observation that some of the tested discs contained defects prior to loading, while others developed similar morphologies under mechanical loading, provides insight into potential mechanisms of degeneration. While degeneration does not always lead to herniation (Lama *et al.*, 2013), it has been suggested that early stage degeneration weakens the disc wall by a combination of mechanical and biological factors in a fatigue-type process while the nucleus is still hydrated and thus able to generate substantial pressure, leading to herniation (Adams, 2004; Adams and Dolan, 2012; Adams and Hutton, 1982). The ability of the defects observed in the present study to act as initiation points for herniation supports this hypothesis. They are also consistent with early histological observations by Walmsley of what were termed “degenerative changes” in middle-aged human discs, which appeared to have delamination and disruption of their inner and mid annular wall (Walmsley, 1953). Their development under mechanical loading is also consistent with previous observations of progressive annulus buckling following endplate injuries causing decompression of the nucleus (Adams *et al.*, 2000).

Further support for the mid and inner annulus being susceptible to damage from non-acute loading is found in recent *in vitro* tests, the most recent of which show microstructural damage to this mid and inner annulus region (Schollum *et al.*, 2018; Wade *et al.*, 2016). It is also entirely possible that genetic factors, as implicated in epidemiological studies (Battié *et al.*, 2009), may render some individuals more vulnerable to developing these defects and related degeneration than others. It is considered that the defects observed in the present study are likely associated with long-term occupational type loading in which damage accumulates in the inner

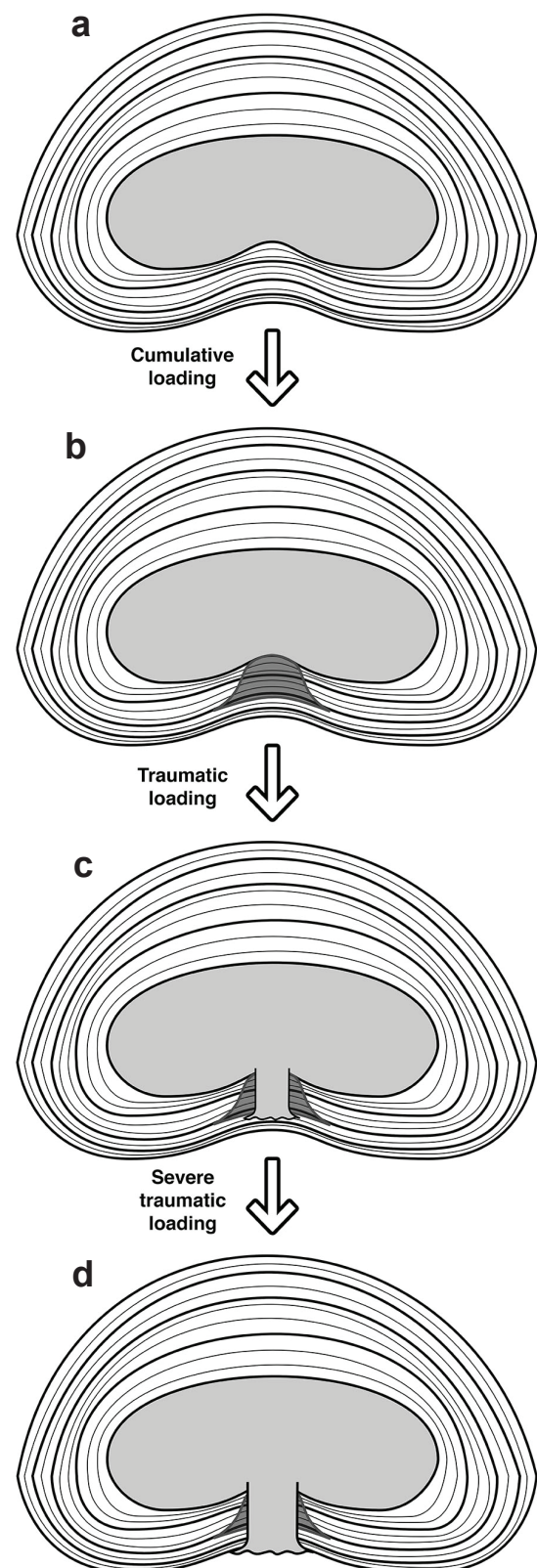


Fig. 6. Schematic representations of the progression/development of characteristic defect in posterior annulus. Beginning with a healthy, regular disc in (a), applied loading causes development of a characteristic defect, as shown in schematic (b). Heavy loading causes displacement of nucleus material into this defect as shown in (c), which can eventually develop into a full-scale herniation as shown in (d), depending on the extent of the defect and severity of applied loading.

and mid annulus, increasing the disc's susceptibility to overload failure, until the nucleus degenerates and loses its internal pressure to the point that this risk is negated.

Rationale for the ovine model

While the usage of ovine specimens restricts the transferability of results directly to humans, it should be noted that the ovine spine is a well-accepted model system due to its strong anatomical (Wilke *et al.*, 1997b) and biomechanical (Schmidt and Reitmaier, 2013; Wilke *et al.*, 1997a) similarities to the human system. In particular, the trabecular structure of the vertebra indicates that both vertebral columns are subject to axial loading (Smit, 2002). Previous *in vitro* studies, using ovine tissue (Berger-Roscher *et al.*, 2017; Wade *et al.*, 2014; Wade *et al.*, 2015; Wade *et al.*, 2016; Wilke *et al.*, 2016), have produced very similar damage morphologies to those carried out using human tissue (Adams and Hutton, 1981; Adams and Hutton, 1982; Adams and Hutton, 1985; Farfan *et al.*, 1970). Given the ready availability of relatively healthy ovine tissue, it is well suited to the current investigation.

How do these defects relate to existing knowledge of disc failure?

It is strongly emphasised that this is not a suggestion that this mechanism is the only way that disc failure can occur; rather, that there are several possible failure mechanisms for the disc and that these are affected by the loading regime the disc is subjected to as well as the structure of the disc! For example, previous studies, notably that by Berger-Roscher *et al.* (Berger-Roscher *et al.*, 2017) and the recent work of van Heeswijk *et al.* (van Heeswijk *et al.*, 2017), both show that disc herniation can occur posterolaterally. This is also commonly observed clinically (Ebeling and Reulen, 1992; Ohshima *et al.*, 1993). It is notable that both these studies were conducted using healthy discs and thus would presumably have excluded discs containing pre-existing defects such as those seen in the present study. It is therefore proposed that herniation involving circumferential tracking or posterolateral failure is more likely in the absence of the characteristic defects observed in the present study, providing a weak point in the annular wall.

The present results also indicate that HR-MRI is capable of detecting discs at risk of suffering herniation. Therefore, while it is possible to suggest that clinical MRI could have the potential to identify individuals at risk of suffering disc herniation, there are obvious practical issues with this. Firstly, these defects must be characterised histologically and microstructurally in order to thoroughly understand their structure, and secondly, that such features can be reliably identified with clinical MRI techniques needs to be shown. Even if this were possible, there would still be the substantial cost associated with performing scans on otherwise healthy patients, and the potential medico-legal issues associated with

any such findings. Given that more advanced disc degeneration would likely negate the risk posed by these defects, it is suggested that these findings reinforce the importance of proper manual handling techniques and spine health in order to avoid acute overloading situations that could cause failure of vulnerable discs.

Conclusions

This study directly showed that naturally occurring pre-existing disc structure can increase vulnerability to herniation. The results indicated that the pre-existing characteristic bell-shaped defects, observed prior to testing in the dorsal annulus, acted as initiation sites for nucleus displacement in the discs that failed in this study. Mechanical loading also produced similar defects, further implicating this factor in the development of disc degeneration although biological and genetic factors would also be involved *in vivo*.

Acknowledgements

We gratefully acknowledge funding from the German Research Foundation (DFG) Project WI 1352/14-3. Dr. Wade gratefully acknowledges funding from the Alexander von Humboldt Foundation. The authors would like to thank the Ulm University Centre for Translational Imaging MoMAN for its support. We thank Anne Subgang, Marija Josipovic and Laura Schmidt for their assistance in preparing and scanning the discs.

References

- Adams MA (2004) Biomechanics of back pain. *Acupunct Med* **22**: 178-188.
- Adams MA, Dolan P (2012) Intervertebral disc degeneration: evidence for two distinct phenotypes. *J Anat* **221**: 497-506.
- Adams MA, Freeman BJC, Morrison HP, Nelson IW, Dolan P (2000) Mechanical initiation of intervertebral disc degeneration. *Spine (Phila Pa 1976)* **25**: 1625-1636.
- Adams MA, Hutton WC (1981) The relevance of torsion to the mechanical derangement of the lumbar spine. *Spine (Phila Pa 1976)* **6**: 241-248.
- Adams MA, Hutton WC (1982) Prolapsed intervertebral disc: A hyperflexion injury. *Spine (Phila Pa 1976)* **7**: 184-191.
- Adams MA, Hutton WC (1985) Gradual disc prolapse. *Spine (Phila Pa 1976)* **10**: 524-531.
- Battié MC, Videman T, Kaprio J, Gibbons LE, Gill K, Manninen H, Saarela J, Peltonen L (2009) The Twin Spine Study: Contributions to a changing view of disc degeneration. *Spine J* **9**: 47-59.

- Berger-Roscher N, Casaroli G, Rasche V, Villa T, Galbusera F, Wilke HJ (2017) Influence of complex loading conditions on intervertebral disc failure. *Spine (Phila Pa 1976)* **42**: E78-E85.
- Berger-Roscher N, Galbusera F, Rasche V, Wilke HJ (2015) Intervertebral disc lesions: visualisation with ultra-high field MRI at 11.7 T. *Eur Spine J* **24**: 2488-2495.
- Callaghan JP, McGill SM (2001) Intervertebral disc herniation: Studies on a porcine model exposed to highly repetitive flexion/extension motion with compressive force. *Clin Biomech (Bristol, Avon)* **16**: 28-37.
- Casaroli G, Villa T, Bassani T, Berger-Roscher N, Wilke HJ, Galbusera F (2017) Numerical prediction of the mechanical failure of the intervertebral disc under complex loading conditions. *Materials (Basel)* **10**: 31.
- Consmuller T, Rohlmann A, Weinland D, Druschel C, Duda G, Taylor, W. (2012) Velocity of lordosis angle during spinal flexion and extension. *PLoS One* **7**: e50135. DOI: 10.1371/journal.pone.0050135.
- Dolan P, Adams MA (1993) The relationship between EMG activity and extensor moment generation in the erector spinae muscles during bending and lifting activities. *J Biomech* **26**: 513-522.
- Ebeling U, Reulen HJ (1992) Are there typical localisations of lumbar disc herniations? A prospective study. *Acta Neurochir (Wien)* **117**: 143-148.
- Fardon DF, Williams AL, Dohring EJ, Murtagh FR, Gabriel Rothman SL, Sze GK (2014) Lumbar disc nomenclature: version 2.0: Recommendations of the combined task forces of the North American Spine Society, the American Society of Spine Radiology and the American Society of Neuroradiology. *Spine J* **14**: 2525-2545.
- Farfan HF, Cossette, J.W., Robertson, G.H., Wells, R.V., Kraus, H. (1970) The effects of torsion on the lumbar intervertebral joints: the Role of torsion in the production of disc degeneration. *J Bone Joint Surg Am* **52**: 468-497.
- Gregory DE, Callaghan JP (2011) Does vibration influence the initiation of intervertebral disc herniation?: an examination of herniation occurrence using a porcine cervical disc model. *Spine (Phila Pa 1976)* **36**: E225-E231.
- Kandel R, Roberts S, Urban JPG (2008) Tissue engineering and the intervertebral disc: the challenges. *Eur Spine J* **17 Suppl 4**: S480-S491.
- Lama P, Le Maitre CL, Dolan P, Tarlton JF, Harding IJ, Adams MA (2013) Do intervertebral discs degenerate before they herniate, or after? *Bone Joint J* **95 B**: 1127-1133.
- Moore RJ, Vernon-Roberts B, Fraser RD, Osti OL, Schembri M (1996) The origin and fate of herniated lumbar intervertebral disc tissue. *Spine (Phila Pa 1976)* **21**: 2149-2155.
- Nachemson A (1960) Lumbar intradiscal pressure. Experimental studies on post-mortem material. *Acta Orthop Scand Suppl* **43**: 1-104.
- Neidlinger-Wilke C, Galbusera F, Pratsinis H, Mavrogonatou E, Mietsch A, Kleisas D, Wilke H-J (2014) Mechanical loading of the intervertebral disc: from the macroscopic to the cellular level. *Eur Spine J* **23 Suppl 3**: 333-343.
- Ohshima H, Hirano N, Osada R, Matsui H, Tsuji H (1993) Morphologic variation of lumbar posterior longitudinal ligament and the modality of disc herniation. *Spine (Phila Pa 1976)* **18**: 2408-2411.
- Panjabi MM, Krag M, Summers D, Videman T (1985) Biomechanical time-tolerance of fresh cadaveric human spine specimens. *J Orthop Res* **3**: 292-300.
- Pearcy MJ, Bogduk N (1988) Instantaneous axes of rotation of the lumbar intervertebral joints. *Spine (Phila Pa 1976)* **13**: 1033-1041.
- Rajasekaran S, Bajaj N, Tubaki V, Kanna RM, Shetty AP (2013) ISSLS prize winner: the anatomy of failure in lumbar disc herniation: an *in-vivo*, multimodal, prospective study of 181 subjects. *Spine (Phila Pa 1976)* **38**: 1491-1500.
- Reitmaier S, Schmidt H, Ihler R, Kocak T, Graf N, Ignatius A, Wilke HJ (2013) Preliminary investigations on intradiscal pressures during daily activities: an *in vivo* study using the merino sheep. *PLoS One* **8**: e69610. DOI: 10.1371/journal.pone.0069610.
- Roaf R (1960) A study of the mechanics of spinal injuries. *J Bone Joint Surg Br* **42B**: 810-823.
- Schmidt H, Kettler A, Heuer F, Simon U, Claes L, Wilke HJ (2007a) Intradiscal pressure, shear strain, and fiber strain in the intervertebral disc under combined loading. *Spine (Phila Pa 1976)* **32**: 748-755.
- Schmidt H, Kettler A, Rohlmann A, Claes L, Wilke HJ (2007b) The risk of disc prolapses with complex loading in different degrees of disc degeneration - a finite element analysis. *Clin Biomech (Bristol, Avon)* **22**: 988-998.
- Schmidt H, Reitmaier S (2013) Is the ovine intervertebral disc a small human one? A finite element model study. *J Mech Behav Biomed Mater* **17**: 229-241.
- Schollum ML, Wade KR, Robertson PA, Thambyah A, Broom ND (2018) A microstructural investigation of disc disruption induced by low frequency cyclic loading. *Spine (Phila Pa 1976)* **43**: E132-E142.
- Shan Z, Wade KR, Schollum ML, Robertson PA, Thambyah A, Broom ND (2017) A more realistic disc herniation model incorporating compression, flexion and facet-constrained shear: a mechanical and microstructural analysis. Part II: high rate or 'surprise' loading. *Eur Spine J* **26**: 2629-2641.
- Sivan SS, Hayes AJ, Wachtel E, Catterson B, Merkher Y, Maroudas A, Brown S, Roberts S (2014) Biochemical composition and turnover of the extracellular matrix of the normal and degenerate intervertebral disc. *Eur Spine J* **23**: 344-353.
- Smeathers JE, Joanes, D. N. (1988) Dynamic compressive properties of human lumbar intervertebral joints: a comparison between fresh and thawed specimens. *J Biomech* **21**: 425-433.

Smit TH (2002) The use of a quadruped as an *in vivo* model for the study of the spine - biomechanical considerations. *Eur Spine J* **11**: 137-144.

van Heeswijk VM, Thambyah A, Robertson PA, Broom ND (2017) Posterolateral disc prolapse in flexion initiated by lateral inner annular failure: an investigation of the herniation pathway. *Spine (Phila Pa 1976)* **42**: 1604-1613.

Veres SP, Robertson PA, Broom ND (2009) The morphology of acute disc herniation: a clinically relevant model defining the role of flexion. *Spine (Phila Pa 1976)* **34**: 2288-2296.

Veres SP, Robertson PA, Broom ND (2010a) The influence of torsion on disc herniation when combined with flexion. *Eur Spine J* **19**: 1468-1478.

Veres SP, Robertson PA, Broom ND (2010b) ISSLS prize winner: how loading rate influences disc failure mechanics: a microstructural assessment of internal disruption. *Spine (Phila Pa 1976)* **35**: 1897-1908.

Wade KR, Robertson PA, Thambyah A, Broom ND (2014) How healthy discs herniate: a biomechanical and microstructural study investigating the combined effects of compression rate and flexion. *Spine (Phila Pa 1976)* **39**: 1018-1028.

Wade KR, Robertson PA, Thambyah A, Broom ND (2015) "Surprise" loading in flexion increases the risk of disc herniation due to annulus-endplate junction failure: a mechanical and microstructural investigation. *Spine (Phila Pa 1976)* **40**: 891-901.

Wade KR, Robertson, P.A., Broom, N.D (2014) Influence of maturity on nucleus and endplate integration in the ovine lumbar spine. *Eur Spine J* **4**: 732-744.

Wade KR, Schollum ML, Robertson PA, Thambyah A, Broom ND (2016) ISSLS prize winner: vibration really does disrupt the disc: a microanatomical investigation. *Spine (Phila Pa 1976)* **41**: 1185-1198.

Wade KR, Schollum ML, Robertson PA, Thambyah A, Broom ND (2017) A more realistic disc herniation model incorporating compression, flexion and facet-constrained shear: a mechanical and microstructural analysis. Part I: Low rate loading. *Eur Spine J* **26**: 2616-2628.

Walmsley R (1953) The development and growth of the intervertebral disc. *Edinb Med J* **60**: 341-364.

Wilke H-J, Jungkunz B, Wenger K, Claes LE (1998) Spinal segment range of motion as a function of *in vitro* test conditions: effects of exposure period, accumulated cycles, angular-deformation rate, and moisture condition. *Anat Rec* **251**: 15-19.

Wilke HJ, Kettler A, Claes LE (1997a) Are sheep spines a valid biomechanical model for human spines? *Spine (Phila Pa 1976)* **22**: 2365-2374.

Wilke HJ, Kettler A, Wenger KH, Claes LE (1997b) Anatomy of the sheep spine and its comparison to the human spine. *Anat Rec* **247**: 542-555.

Wilke HJ, Kienle A, Maile S, Rasche V, Berger-Roscher N (2016) A new dynamic six degrees of freedom disc-loading simulator allows to provoke disc damage and herniation. *Eur Spine J* **25**: 1363-1372.

Yates JP, McGill SM (2011) The effect of vibration and posture on the progression of intervertebral disc herniation. *Spine (Phila Pa 1976)* **36**: 386-392.

Yoshioka T, Tsuji H, Hirano N, Sainoh S (1990) Motion characteristic of the normal lumbar spine in young adults: Instantaneous axis of rotation and vertebral center motion analyses. *J Spinal Disord* **3**: 103-113.

Supplementary videos details

(Available on paper website)

Video 1. 2498 L4-5. Group 2 (no lateral bending), Cycles 60-100 shown. Audible snapping sounds accompany the appearance of a wrinkle in the dorsal longitudinal ligament, indicating that the annulus wall beneath it is distorting. With increasing cycles, the wrinkle becomes more prominent. This disc suffered subligamentous herniation when assessed by HR-MRI.

Video 2. 2498 L5-6. Group 1 (no flexion), Cycles 50-130 shown. Audible snapping sounds accompany the appearance of a wrinkle in the dorsal longitudinal ligament, which progressively bulges and ruptures with increasing cycles. This disc suffered a prominent herniation when assessed by HR-MRI.

Video 3. 2496 L4-5. Group 4 (all components combined), Cycles 60-120 shown. Audible snapping sounds accompany irregular bulging in the dorsal annulus wall, suggesting that it is being progressively distorted and disrupted as cycle numbers increase. This disc suffered subligamentous herniation when assessed by HR-MRI.

Video 4. 2496 L5-6. Group 5 (all components combined), Cycles 0-60 shown. Each component of posture is applied simultaneously prior to cycling. As this occurs, the dorsal wall of the annulus can be seen to partially rupture. As load is progressively applied, nucleus material is extruded through this rupture. As would be expected, this disc had suffered a prominent herniation when assessed by HR-MRI.

Editor's note: There were no questions from reviewers for this paper, so there is no Discussion with Reviewers section. The Scientific Editor responsible for this paper was Sibylle Grad.